BOLETÍN DE LA SOCIEDAD ESPAÑOLA DE CERÁMICA Y VIDRIO xxx (2023) xxx–xxx

BOLETIN DE LA SOCIEDAD ESPAÑOLA DE
Cerámica y Vidrio
www.elsevier.es/bsecv

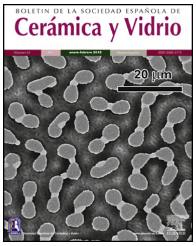

Original

Synthesis and characterisation of hybrids composed of calcined hydrotalcite and residual textile dyes

Daniel López-Rodríguez[a,*], *Jorge Jordan-Nuñez*[b], *Bàrbara Micó-Vicent*[b], *Raúl Llinares Llopis*[c], *María Moncho-Santonja*[d]

[a] *Departamento de Ingeniería Textil y Papelera, Universitat Politècnica de València, Plaza Ferrándiz y Carbonell s/n, Alcoi, Spain*
[b] *Departamento de Ingeniería Gráfica, Universitat Politècnica de València, Plaza Ferrándiz y Carbonell s/n, Alcoi, Spain*
[c] *Departamento de Comunicaciones, Universitat Politècnica de València, Plaza Ferrándiz y Carbonell s/n, Alcoi, Spain*
[d] *Research Center in Graphical Technologies, Universitat Politècnica de València, Valencia, Spain*

ARTICLE INFO

Article history:
Received 19 July 2023
Accepted 28 September 2023
Available online xxx

Keywords:
Hydrotalcite
Dye adsorption
Clay pigment
Direct dye recovery
Removal of dyes
Reactive dye recovery
Hybrid pigments
TGA
FTIR
XRD

ABSTRACT

There is growing concern about the health of our planet, which has led to a search for methods to purify and recover the pollutant materials that are released into the environment. Among all industries, the dyeing sector of the textile industry is considered one of the most polluting. However, advancements in technology, such as the use of nanoadsorbents, have made it possible to effectively treat and clean these wastewaters by harnessing the adsorption capabilities of these minerals. As a result, highly functional pigmentary hybrids with improved characteristics can be obtained. In this study, the research focuses on exploring the potential of hydrotalcite in combination with reactive, disperse, and direct dyes. Colour measurements are conducted using reflection spectrophotometers to evaluate the colour performance of the hybrid materials, yielding successful results. X-ray diffraction (XRD) analysis is used to verify the structural integrity of the hydrotalcite and confirm the adsorption of the dyes. Additionally, thermogravimetric tests (TGA) are carried out to assess the thermal stability of the different samples, while the colorants' protection provided by the hydrotalcite is evaluated through total soluble recovery (TSR) measurements. An FTIR analysis is used to detect the presence of characteristic functional groups of the dyes in the resulting hybrids. Surface area and porosity measurements utilising the BET method, along with Scanning Electron Microscopy Energy + Dispersive X-ray spectroscopy (SEM–EDX) and X-ray photoelectron spectroscopy (XPS) tests, are also conducted. In summary, this study investigates the potential of hydrotalcite as an effective adsorbent for various dyes used in the textile industry. The research involves comprehensive analyses, including colour evaluation, structural characterisation, thermal stability assessment, and surface morphology examination. These findings contribute to the development of sustainable and environmentally friendly approaches in the treatment of textile wastewater.

---

* *Corresponding author.*
E-mail address: dalorod@upv.es (D. López-Rodríguez).

https://doi.org/10.1016/j.bsecv.2023.09.003

Please cite this article in press as: D. López-Rodríguez, et al., Synthesis and characterisation of hybrids composed of calcined hydrotalcite and residual textile dyes, Bol. Soc. Esp. Cerám. Vidr. (2023), https://doi.org/10.1016/j.bsecv.2023.09.003

Síntesis y caracterización de híbridos compuestos de hidrotalcita calcinada y colorantes textiles residuales

Palabras clave:
Hidrotalcita
Adsorción de colorantes
Pigmento arcilloso
Recuperación directa de colorantes
Eliminación de colorantes
Recuperación de colorantes reactivos
Pigmentos híbridos
TGA
FTIR
DRX

RESUMEN

La preocupación por la salud de nuestro planeta es cada vez mayor, lo que ha llevado a buscar métodos para depurar y recuperar los materiales contaminantes que se vierten al medio ambiente. Entre todas las industrias, el sector de la tintura de la industria textil se considera uno de los más contaminantes. Sin embargo, los avances tecnológicos, como el uso de nanoadsorbentes, han permitido tratar y limpiar eficazmente estas aguas residuales aprovechando la capacidad de adsorción de estos minerales. Como resultado, se pueden obtener híbridos pigmentarios altamente funcionales con características mejoradas. En este estudio, la investigación se centra en explorar el potencial de la hidrotalcita en combinación con colorantes reactivos, dispersos y directos. Se llevan a cabo mediciones del color utilizando espectrofotómetros de reflexión para evaluar el rendimiento cromático de los materiales híbridos, obteniéndose resultados satisfactorios. El análisis de difracción de rayos X (DRX) se utiliza para verificar la integridad estructural de la hidrotalcita y confirmar la adsorción de los colorantes. Además, se llevan a cabo ensayos termogravimétricos (TGA) para evaluar la estabilidad térmica de las diferentes muestras, mientras que la protección de los colorantes proporcionada por la hidrotalcita se evalúa mediante mediciones de reflectancia solar total (TSR). Se utiliza un análisis FTIR para detectar la presencia de grupos funcionales característicos de los colorantes en los híbridos resultantes. También se realizan mediciones del área superficial y la porosidad utilizando el método BET, junto con ensayos de espectroscopia de rayos X de energía + dispersión por microscopía electrónica de barrido (SEM-EDX) y espectroscopia de fotoelectrones de rayos X (XPS). En resumen, este estudio investiga el potencial de la hidrotalcita como adsorbente eficaz para diversos colorantes utilizados en la industria textil. La investigación incluye análisis exhaustivos, como la evaluación del color, la caracterización estructural, la evaluación de la estabilidad térmica y el examen de la morfología superficial. Estos resultados contribuyen al desarrollo de enfoques sostenibles y respetuosos con el medio ambiente en el tratamiento de aguas residuales textiles.

Introduction

In recent years, concerns about environmental pollution caused by the textile industry [1–3] have increased significantly. The release of residual dyes in textile wastewater has been identified as a major source of water pollution, due to their toxicity and resistance to biological degradation. Consequently, the search for efficient and sustainable methods to treat textile effluents and minimise their impact on the environment has become a priority.

In this context, hybrid materials composed of calcined hydrotalcite [4–6] have emerged as a promising alternative for the removal of residual dyes in textile wastewater. Hydrotalcite is a composite of double sheets of metal hydroxides with anion exchange capacity, while calcination refers to the process of heating at high temperature to obtain highly dispersed metal oxides. These materials combine the adsorption properties of hydrotalcite with the catalytic capabilities of metal oxides, giving them high efficiency in dye degradation.

The aim of this study is to synthesise and characterise calcined hydrotalcite composite hybrids and to evaluate their ability to adsorb and degrade textile residual dyes present in wastewater. To achieve this objective, different synthesis methods will be used and the influence of the synthesis conditions on the properties and characteristics of the hybrids obtained will be investigated. Furthermore, the adsorption properties and degradation mechanisms of the dyes in the presence of the composite hybrids will be analysed. Given the objective of our work, in order to assess the suitability of hydrotalcite for use as an adsorbent for textile dyes, we will need the simulated wastewater containing the dye to be free of the dye, which will be assessed by absorbance readings in the transmission spectrophotometer.

The contribution of this study lies in the synthesis and characterisation of calcined hydrotalcite composite hybrids with potential applicability in the removal of residual dyes from textile wastewater. It is expected that the results obtained will provide a better understanding of the dye adsorption and degradation processes, as well as the optimisation of the synthesis conditions to improve the efficiency of the hybrid materials in environmental applications.

In summary, this article presents a detailed investigation on the synthesis and characterisation of calcined hydrotalcite composite hybrids and their ability to adsorb and degrade textile waste dyes. The results obtained will contribute to the

Please cite this article in press as: D. López-Rodríguez, et al., Synthesis and characterisation of hybrids composed of calcined hydrotalcite and residual textile dyes, Bol. Soc. Esp. Cerám. Vidr. (2023), https://doi.org/10.1016/j.bsecv.2023.09.003

development of sustainable methods for the treatment of textile wastewater, offering a promising approach to address the environmental problems associated with dye pollution.

Hydrotalcite-type nanoadsorbents, also known as layered double hydroxides (LDH), are of great interest to the scientific community thanks to their use as nanoadsorbents, pharmaceuticals or catalysers, among others [7]. The crystalline structure of this clay is based on the positive charge of its layers which are compensated by the intercalated layers with negative charges of certain anions such as carbonate and water molecules [8–10]. Researchers are showing increasing interest in such elements thanks to their wide range of applications as catalysts, and also in medicine, adsorption, etc. [7]. Different methods exist by means of which the adsorption of anions by LDH composites takes place. The most common one is that produced by direct adsorption in dispersion. A solid's crystallinity limits such adsorption for the following reasons: the medium's polarity, temperature, anion size, and pH [11–13]. The second, albeit slightly more time-consuming, method, but one offering clear advantages, is calcining. Former studies have demonstrated that hydrotalcite has shape memory after being exposed to a high thermal source. This substantially changes its initial laminar arrangement, which recovers during later hydration processes. After being exposed to temperatures of 450–550 °C, it is reconstructed as previously described thanks to the anions present in dissolution and their incorporation into the new nanoclay structure [14–16].

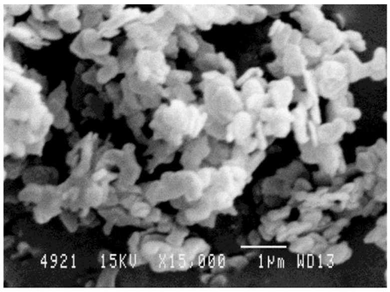

The aim of this work is to synthesise coloured compounds obtained from the adsorption of dyes discharged in textile wastewater by LDH. There are different ways to use hydrotalcite: by coprecipitation [17], direct application [11–13] or calcination [14–16].

Materials and methods

Hydrotalcite (LDH) $Mg_6Al_2(CO_3)(OH)_{16}\cdot4(H_2O)$ [11–13] has been selected as an adsorbent substance for the dyes. The hydrotalcite used in this work was purchased from the commercial distributor Merck. In this study, the calcination of hydrotalcite was carried out according to the method proposed by Dos Santos R.M.M. [18], which resulted in the destruction of its structure and facilitated the penetration of the dye into the nanoadsorbent. A 100 g sample of hydrotalcite is taken and placed in a muffle for 3 h at 500 °C. It is left to cool in a desiccator so that it does not absorb moisture and is kept in the desiccator until it is used. The laboratory conditions for adsorption and reconstruction were 20 °C and 65% humidity. The water used was previously deionised, maintaining a conductivity between 0.2 and 0.8 μS/cm and complying with the requirements of the ISO 3696: 1999 standard. Once immersed in an aqueous solution, the LDH reattained its original structure through its shape memory, thus incorporating the dye into the new structure. Fig. 1 shows images of the nanoadsorbent, where the differences between the hydrotalcite before and after the calcination process are clearly visible. From a morphological point of view, the figures show that the structure of the clay has recovered after the reconstruction. This reconstruction process takes place thanks to the clay's ability to recover its initial shape by rehydration [19].

Three types of dyes of different natures have been used for this research: a direct anionic dye, Direct Blue 199 CI 74180 (DB199) [20] (source: Clariant); a reactive anionic dye, Drimarene Yellow K-2R (RYD) [21] (source: Clariant); and finally,

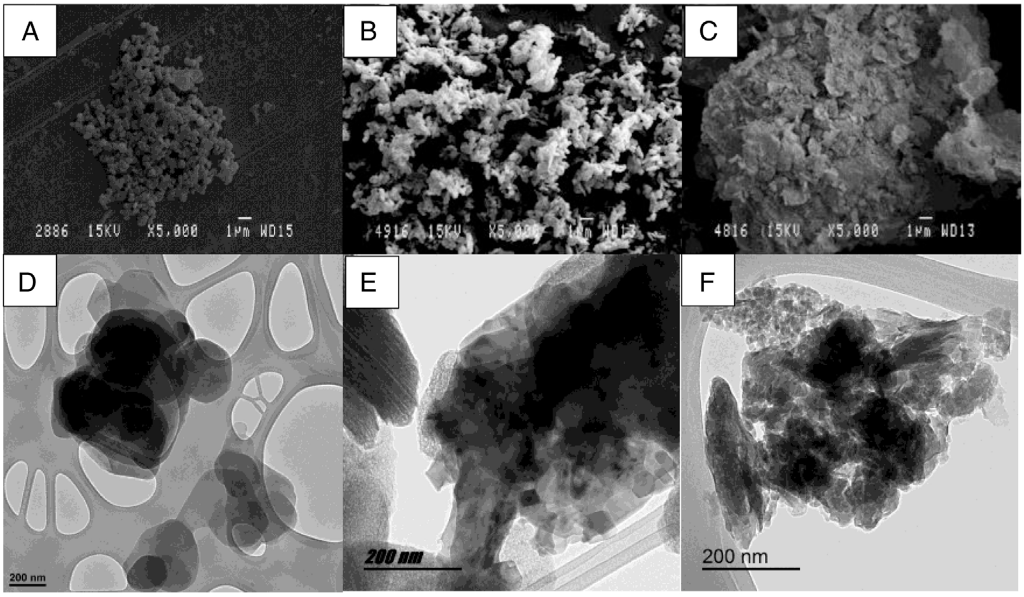

Fig. 1 – SEM micrographs of different HC samples: (a) HC original, (b) HC calcinated, (c) HC reconstructed. TEM micrographs of different HC samples: (d) HC original, (e) HC calcinated, (f) HC reconstructed.

Please cite this article in press as: D. López-Rodríguez, et al., Synthesis and characterisation of hybrids composed of calcined hydrotalcite and residual textile dyes, Bol. Soc. Esp. Cerám. Vidr. (2023), https://doi.org/10.1016/j.bsecv.2023.09.003

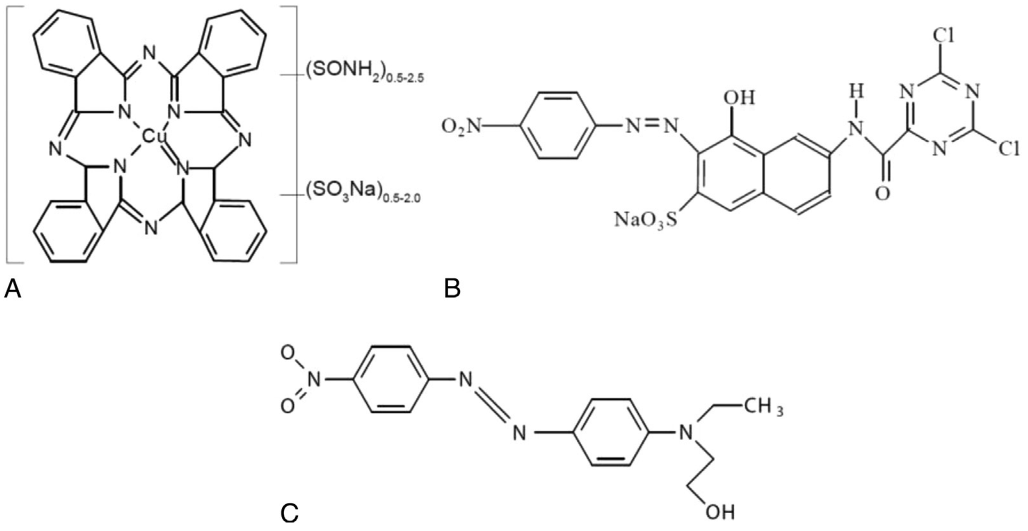

Fig. 2 – (a) Direct Blue 199 [20], (b) Reactive Drimarene Yellow [21], (c) Disperse Red 1 [22].

Table 1 – Lambert–Beer line equations and R^2.

Dye	Equation	R^2
Direct Blue 199 (DB199)	$y = 21.784\ x - 0.015$	0.9982
Reactive Yellow (RYD)	$y = 14.943\ x - 0.0021$	0.9993
Disperse Red 1 (DR1)	$y = 25.411\ x - 0.0244$	0.9989

Disperse Red 1 CI 11110 (DR1) [22] (source: Clariant) was used as a non-ionic disperse dye. Fig. 2 shows the chemical structures of each of these dyes.

In order to determine the concentration of dye remaining in a dye bath after LDH adsorption, it will be necessary to generate Lambert–Beer curves [23] to calculate this concentration in aqueous solution. To achieve this, multiple readings will be made in a transmission spectrophotometer using different dye solutions with known concentrations. The data obtained will be used to establish the equations shown in Table 1.

The main objective of this study is to achieve maximum adsorption of the dyes by the HC clay, leaving the water free of contaminants. In the experimental phase of adsorption, solutions of each dye are prepared with a concentration of 1 g L^{-1}, using a total volume of 3 l. Immediately afterwards, 3 g L^{-1} of hydrotalcite is added to each solution. The mixture is then stirred using a magnetic stirrer, which operates at 1600 rpm for the first two hours and then reduces its speed to 600 rpm. This configuration allows for a first adsorption stage [24], in which the penetration of the dye is favoured due to a higher centrifugal force. Subsequently, it is ensured that the dye is not released from the clay, which is why the speed is reduced in an “ageing” stage of the hybrid formed. After the above-mentioned time has elapsed, the solution is filtered to separate and collect the LDH from the aqueous solution. Filter paper is used and allowed to stand for 48 h to allow the water to dissipate by gravity and separate from the clay. The water is then sampled, and a new reading is taken using the transmission spectrophotometer. Using the equations in Table 1, the concentration of dye that remains in the water and has not been adsorbed is calculated [25,26]. The clay on the filter paper is collected and freeze-dried to remove any water that may have been adsorbed [27,28] to remove any residual water present in the HC.

To measure the colour of the clay-dye hybrids and the total solar reflectance (TSR) [29], a Jasco V-670 dual UV–VIS/NIR spectrophotometer was used, which operates in the range of 2700–190 nm with a resolution of 0.5 nm. This instrument has a double grating monochromator. The first grating is used for the UV–VIS range with a resolution of 1200 grids-mm^{-1} and detectors based on a photomultiplier tube. The second grating is used for the infrared (IR) region with a resolution of 300 lines/mm and a PbS detector. Both the first and the second detector have an automation system that manages the changes and adjusts them according to the wavelength required at any given moment. A halogen lamp (330–2700 nm) and a deuterium lamp (190–350 nm) were used as light sources. Reflectance factors for the hybrid pigments were applied with the CIE-1964 observer and D65 illumination to obtain optical property values and make comparisons [30]. For these colour measurements, the samples are placed directly into a sample capsule and a diffuse reflectance measurement is performed.

A scanning electron microscope (SEM) model PHENOM (FEI Company, Eindhoven, The Netherlands) with an electron acceleration of 5 kV was used to carry out the topographical analysis of the surface of the samples. Prior to this, the samples were sputter coated with a gold-palladium alloy using an EMITECH sputter coater mod. SC7620 (Quorum Technologies Ltd., East Sussex, UK). The coating, with a thickness of only 5–7 nm, does not affect the results obtained.

To evaluate the thermal properties of the hybrids, thermogravimetric analysis (TGA) was performed to compare the variation in the degradation peaks of the dyes and clay-dye composites [31–33]. The analysis was carried out using a TGA/SDTA 851 thermogravimetric analyser (Mettler-Toledo Inc., Columbus, OH, USA). The experimental conditions established included a temperature increase of 5 °C per minute over a study range of 20–900 °C, using an N_2:O_2 (4:1) atmosphere as the oxidation medium.

For the characterisation of the hybrids, an infrared spectrophotometer was used to obtain the Fourier transform

Please cite this article in press as: D. López-Rodríguez, et al., Synthesis and characterisation of hybrids composed of calcined hydrotalcite and residual textile dyes, Bol. Soc. Esp. Cerám. Vidr. (2023), https://doi.org/10.1016/j.bsecv.2023.09.003

Table 2 – Difference in concentration after LDH adsorption.

Sample ref.	Dye	Initial conc. g L^{-1}	Final conc. g L^{-1}	Ads (%)
1	Direct Blue 199	1	6.55E−04	99.934
2	Reactive Yellow Drimaren	1	5.13E−04	99.949
3	Disperse Red 1	1	6.21E−03	99.938

Table 3 – L^*, a^*, b^*, C^*_{ab} values of each dye and each hybrid.

Sample	L^*	a^*	b^*	C^*_{ab}	h
DB199	44.94	2.03	−1.88	2.77	317.16
RYD	50.96	5.79	11.08	12.50	62.39
DR1	50.77	15.14	5.86	16.24	21.17
4	56.09	−1.77	−15.03	15.14	263.30
5	86.21	−8.75	42.61	43.50	101.61
6	50.77	15.14	5.86	16.24	21.17
H	97.01	0	3.65	3.65	90
HC	94.25	0	1.88	1.88	90

(FTIR). Given the material to be studied, a horizontal attenuated total reflection (FTIR–ATR) using a ZnSe prism was used. The equipment used was a Jasco FTIR 4700 IRT 5200 spectrometer equipped with a DTGS detector. Uniform pressure was applied using a pressure fitting on all samples. The spectrum was obtained by 64 scans with a resolution of 4 cm^{-1}.

Subsequently, an X-ray diffraction (XRD) test was carried out to study the changes in the shape and lamellar structure of the LDH before and after calcination and rehydration [34,35]. A Bruker D8-Advance XRD (Bruker, Billerica, MA, USA) with a Göebel mirror (power: 3000 W, voltage: 20–60 kV and current: 5–80 mA) was used. Readings were taken in an oxidising atmosphere with an angular velocity of 1°/min, a step of 0.05° and an angular range of 2.7–70°. This test is of particular importance to analyse the basal space in the hydrotalcite structure resulting from the adsorption of the dyes.

Finally, X-ray photoelectron spectroscopy (XPS) and energy dispersive X-ray spectroscopy coupled to scanning electron microscopy (SEM–EDX) techniques were used to determine and analyse the surface composition and oxidation state. These techniques were applied to both pure hydrotalcite and dye-loaded hybrids in order to study the changes that occurred after dye adsorption.

For the surface analysis, X-ray photoelectron spectroscopy (XPS) was used with the Thermo Scientific NEXSA spectrometer, using monochromatised radiation at 1486.6 eV generated by a double crystal monochromator. A focused X-ray spot with a diameter of 400 μm was produced at a current of 6 mA and a voltage of 12 kV. The alpha hemispherical analyser was used in constant energy mode, with analysis step energies of 200 eV to cover the whole energy band, and 50 eV in a narrow scan to obtain element-specific results. The XPS technique was used to obtain information on the chemical bonding state and surface elemental composition of the samples. Charge compensation was achieved using a flood gun system that generated low-energy electrons and low-energy argon ions from a single source.

Energy dispersive X-ray (EDX) analyses were carried out using a JEOL JSM-6300 scanning electron microscope. All samples were pre-coated with a graphite layer to impart conductivity to the non-conductive surfaces. Non-metallic coatings were used to avoid possible interference in the results. The EDX spectra obtained allowed the elemental composition of the materials deposited on the surface of the hybrids to be determined.

Results and discussion

Hydrotalcite is a synthetic LDH mineral with unique adsorption properties, which enable it to effectively remove dyes in various industrial and environmental applications. Hydrotalcite's ability to adsorb dyes is based on its layered structure and surface charge. When a dye is in aqueous solution, its molecules have an electrical charge that can interact with the surface charge of the hydrotalcite. The hydrotalcite layers have a positive charge, which attracts negatively charged dyes. This electrostatic attraction process allows the hydrotalcite to adsorb the dyes and retain them in its structure.

In addition to electrostatic interaction, hydrotalcite can also adsorb dyes through hydrogen bonds and Van der Waals forces. These additional intermolecular bonds and forces contribute to a stronger and more selective adsorption of the dyes.

Final concentration in solution

After the adsorption process, excellent results were obtained with adsorption percentages above 99% (Table 2), which shows the high capacity of LDH to adsorb dyes used in the textile industry, supporting previous findings [18,36–39]. Both ionic and non-ionic dyes showed almost complete adsorption, with no significant differences in dye loadings. However, differences may be observed in future tests and trials, partly due to the inherent properties of the LDH used.

Hybrid colour measurements

Table 3 and Fig. 3 show the measurements taken to calculate the colour of the three hybrids obtained, represented in a chromatic diagram. To obtain the master colour calculations for each of the hybrid pigments, the reflectance values (λ) of these dye-LDH hybrids were used, following the guidelines of the International Commission on Illumination CIE 15:2004

Please cite this article in press as: D. López-Rodríguez, et al., Synthesis and characterisation of hybrids composed of calcined hydrotalcite and residual textile dyes, Bol. Soc. Esp. Cerám. Vidr. (2023), https://doi.org/10.1016/j.bsecv.2023.09.003

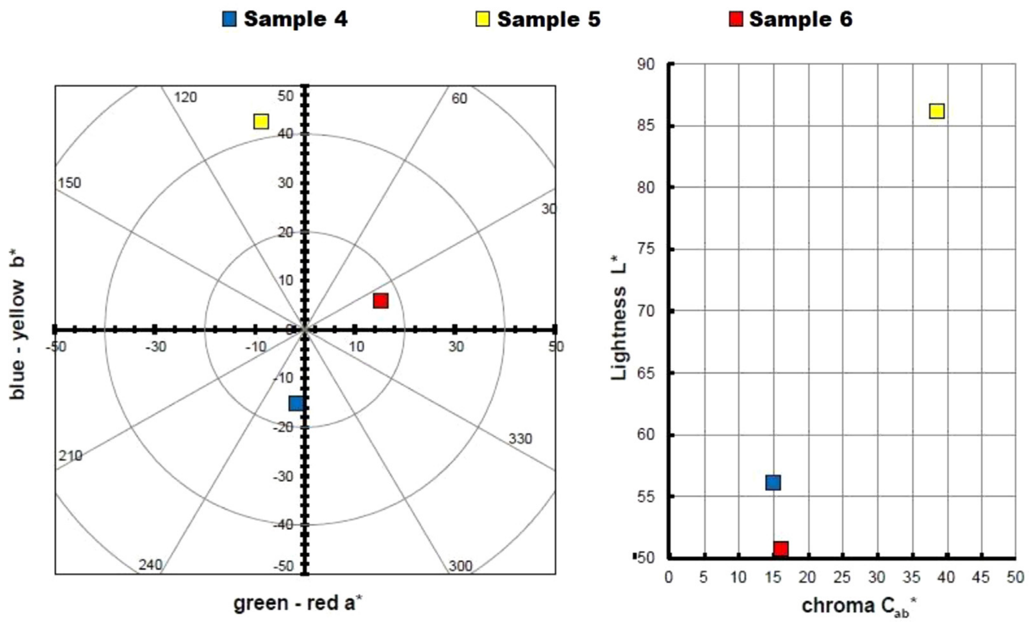

Fig. 3 – Graphic CIELAB plots for hybrid pigments synthesised using the D65 illuminant and the CIE-1931 XYZ standard observer. Left: CIE-*ab** colour diagram; right: CIE-C*ab**L* colour chart.**

[40]. These guidelines allow an objective comparison of absolute and relative colour values using the CIELAB colourimetric parameters, coded by the CIE 1931 XYZ standard and the D65 standard illumination.

The CIE a^*b^* and CIE-Cab^*L^* diagrams in Fig. 3 confirm that the dye removed from the solutions has been trapped in the nanoadsorbent, exhibiting the colours corresponding to the pigments obtained. The yellow hybrid is positioned on the axis and angle characteristic of yellows, with a slight inclination towards greens. The hybrid represented by sample 4 shows a pure blue shade, while the hybrid of sample 6 shows a red shade with a slightly yellowish hue.

Sample 5 is characterised by a higher saturation and luminosity compared to the other two samples, due to the intrinsic properties of yellow that give it a characteristic level of luminosity. This slightly limits the range of colours that could be achieved by increasing or decreasing the amount of dye in the nanoadsorbent. On the other hand, samples 4 and 6 (blue and red respectively) exhibit a much lower luminosity, with an L^* level of 50. These dark, chromatic hybrid pigments offer the possibility of obtaining wider colour ranges by reducing the concentration of the original dyes in the nanoadsorbent.

It is important to mention that the mixture of the three types of hybrid pigments obtained, with colours of such high purity in terms of hue and saturation levels, will considerably widen the range of available colours.

Total solar reflectance (TSR)

When applying certain coatings to a textile substrate, such as in the application of a printing paste, it is essential to consider its behaviour and resistance to various external factors. One of the crucial aspects is the ability of the coating to absorb and reflect light radiation. Therefore, a comprehensive study has been carried out to evaluate this radiation using the total solar reflectance factor (TSR).

Total solar reflectance (TSR) is a parameter used to measure the ability of a material or coating to reflect incident solar radiation. It represents the percentage of solar radiation that is reflected by the surface compared to the total solar radiation incident on it. In simpler terms, total solar reflectance indicates the amount of sunlight that is reflected by a material rather than absorbed. A high TSR value means that the material has a greater ability to reflect solar radiation, resulting in less heat absorption and a lower surface temperature.

Total solar reflectance is calculated using sunlight reflectance measurements of the material in question. These measurements are made considering a wide range of wavelengths to cover the full spectrum of solar radiation. A solar weighting factor is then applied to each wavelength to account for the spectral distribution of solar radiation.

Total solar reflectance is an important parameter in the evaluation of materials used in applications where reduced heat absorption is desired, such as roof coatings, building envelopes or solar shading fabrics. A high TSR can contribute to energy efficiency by helping to maintain lower temperatures on surfaces exposed to the sun and reduce the cooling load. These calculations follow the guidelines established in ASTM G173-03 [41].

A comparative analysis of the total solar reflectance (TSR) assessment for each hybrid and dye studied is presented in Table 4. Upon adsorption of the dye, the white LDH takes on a different hue, resulting in a material with a higher L^* luminosity that will reflect a greater amount of light. When comparing each dye with its corresponding hybrid, an increase in TSR value is observed.

If we examine the comparisons between the hybrids, considering the L^* luminosity values shown in Fig. 4, we highlight sample 5 as the one with an exceptionally high value, both

Please cite this article in press as: D. López-Rodríguez, et al., Synthesis and characterisation of hybrids composed of calcined hydrotalcite and residual textile dyes, Bol. Soc. Esp. Cerám. Vidr. (2023), https://doi.org/10.1016/j.bsecv.2023.09.003

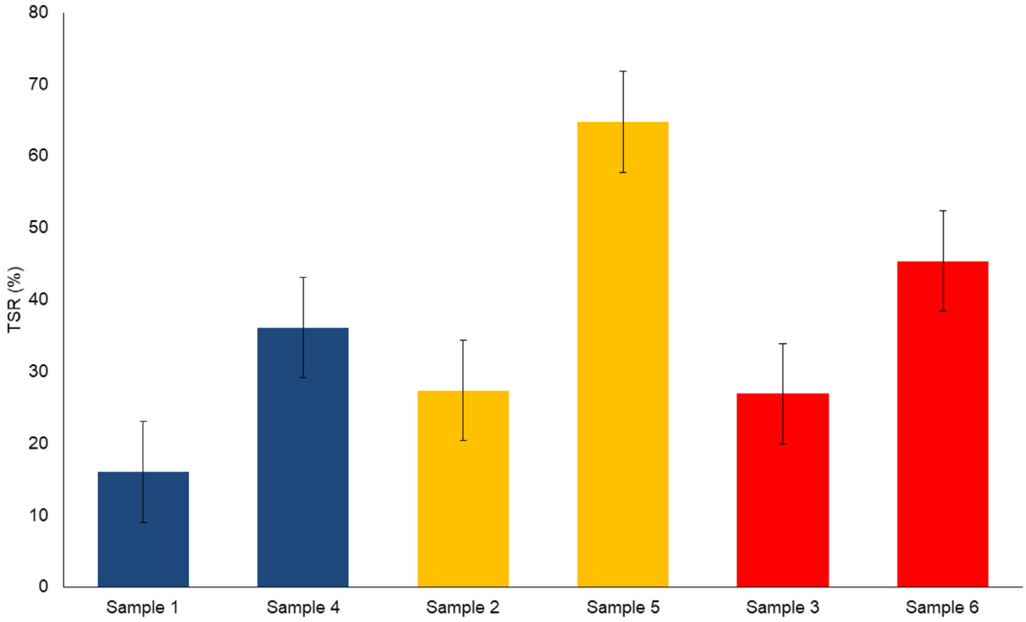

Fig. 4 – Total solar reflectance (TSR (%)) for each sample.

Table 4 – TSR values.

Colouring matter	Sample ref.	TSR %
Direct Blue 199	1	16.05
Reactive Yellow Drimaren K-2R	2	27.38
Disperse Red 1	3	26.93
Hydrotalcite + Direct Blue 199	4	36.14
Hydrotalcite + Reactive Yellow Drimaren K-2R	5	64.77
Hydrotalcite + Disperse Red 1	6	45.40

in TSR and luminosity. As for the second dye and hybrid, the red sample has a higher L^* value compared to the blue sample. In all cases, significant differences are observed between the TSR% values of the original dye and the hybrids obtained. These results are presented visually in Fig. 4, where the pairs of samples are compared according to the corresponding dye.

This information allows us to evaluate and compare the capacity of the different hybrids in terms of their total solar reflectance, which is relevant for applications where the aim is to maximise the reflection of solar radiation and reduce heat absorption.

Fig. 5 shows the reflectance results obtained for each of the hybrids as a function of wavelength. In the ultraviolet (UV) region, hybrids 4 and 6 exhibit very similar behaviour, but hybrid 5 shows significant differences. As we move into the visible spectrum (400–700 nm) and the near infrared (NIR) up to 1200 nm, these differences become more pronounced due to certain chemical properties of each dye and the perception of colour itself (brightness, hue and chroma). However, in the range 1200–1400 nm, the values are quite similar, becoming almost identical in the range of 1400–2400 nm. Therefore, the main discrepancies observed in the TSR values are due to the characteristics of the dyes adsorbed on the nanoadsorbent and their reflectance in both UV–visible and near-infrared up to 1200 nm.

Thermogravimetry (TGA)

Fig. 6 shows the results obtained from the thermogravimetric analysis (TGA). This graphic representation shows, in the upper part, the percentage mass loss of each sample as the temperature increases. In the lower part of the figure, the curves *d*(DB199), *d*(RYD), *d*(DR1), *d*(4), *d*(5), *d*(6) and *d*(H), which are the derivatives (DTGA) of the curves shown in the upper part, can be observed. These derivatives allow a clearer visualisation of the specific degradation peaks that occur.

It is noticeable that the direct and reactive (anionic) dyes exhibit a slower decomposition compared to the disperse dyes. From 500 °C onwards, the anionic dyes in this work no longer experience further degradation, but the non-ionic dye does show a considerable decrease, suffering a degradation of up to 82%. This figure is considerably higher than that of the other two dyes, which reach a maximum degradation of around 49%. These results show that high temperatures affect the disperse dye much more, which can have significant repercussions on colour fastness, as this is affected by situations with high energy inputs, such as ironing or exposure to sunlight.

Fig. 6 presents a comparative study of the reaction of the three dyes individually, the three hybrids and the nanoadsorbent (LHD) alone. For the nanoadsorbent alone (Hydrotalcite), a drop in mass is observed, which is attributed to the evaporation of interlamellar water and physisorbed water in the temperature range between 105 and 168 °C. In addition, another range between 172 and 279 °C can be seen in the graph, which is due to the loss of hydroxyl groups (—OH) in the lamellar layers. Subsequently, a third mass decrease is recorded in the range 275–605 °C, which is attributed to the loss of CO_3^{2-} ions and the combustion of molecular fragments [42–44]. It is worth noting that significant peaks are observed

Please cite this article in press as: D. López-Rodríguez, et al., Synthesis and characterisation of hybrids composed of calcined hydrotalcite and residual textile dyes, Bol. Soc. Esp. Cerám. Vidr. (2023), https://doi.org/10.1016/j.bsecv.2023.09.003

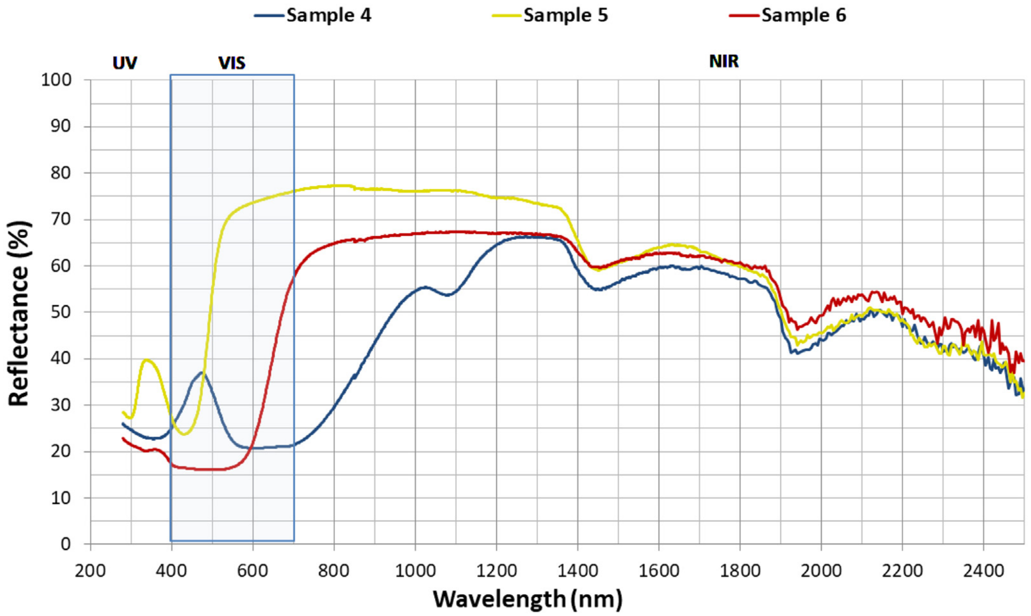

Fig. 5 – TSR (%) for each hybrid.

for hydrotalcite at 208 °C, associated with the loss of interlamellar water, as well as peaks at 297 °C and 411 °C related to the fall of —OH groups [45].

The direct dye B199 shows a noticeable presence of two thermal peaks: one at 414 °C and a much more intense one at 460 °C. However, sample number 4 exhibits a decrease in the intensity of the peaks, making them less prominent and with some displacement as a result of the barrier effect conferred by the nanoadsorbent. Similarly, that the figures show that in this sample, the LDH peak at 208 °C is considerably reduced, adopting a shoulder shape in the range of 160–212 °C. As for the reactive dye RYD, two peaks can be distinguished at 432 and 533 °C, which disappear completely in sample number 5. The shoulder in the 160–212 °C zone continues to show the presence of the LDH peak at 208 °C and also a slightly shifted variation at 297 °C, produced by the evaporation of water from the LHD. On the other hand, the dispersed dye DR1 shows peaks at 283, 427 and 545 °C, the latter being the most prominent and relevant, as it shows a strong degradation at high temperatures, causing a considerable mass loss compared to the other two dyes. After adsorption by LHD, these three peaks have completely disappeared in sample number 6, and in their place the characteristic shoulder in the range of 160–212 °C, typical of the nanoadsorbent appears, as observed in the other samples.

Several research works have revealed that dye-LDH hybrids have experienced a significant increase in their thermal stability due to the effect of hydrotalcite [46,47]. This phenomenon is attributed to two fundamental mechanisms. Firstly, the lamellar structure of the nanoadsorbent provides a protective barrier that limits the volatilisation of the dye components. In addition, when these compounds are subjected to high temperatures, a transfer of energy from the dye to the LDH occurs. Consequently, the nanoadsorbent absorbs this energy, minimising the energetic impact on the dye [48,49]. These discoveries have contributed significantly to the advancement of knowledge in this field.

X-ray diffraction (XRD)

Fig. 7 shows the results of the X-ray diffraction analysis, revealing a distinctive peak in the 11–12° range. This peak corresponds to the curve of uncalcined hydrotalcite. However, when subjected to a calcination process, the disappearance of this peak is observed. This is due to dehydroxylation in the inner layers of the nanoadsorbent [9], which causes the collapse and exfoliation of the lamellar layers. This opening of the lamellar layers that make up the mineral structure plays a crucial role in the penetration of the dye. During the rehydration of the hydrotalcite and its subsequent shape recovery, the LDH incorporates the dye in place of some of its components, such as CO_3^{2-}, thanks to its structural memory capacity [14–16,50].

When further analysing Fig. 7, it is essential to consider the distinction between the amorphous form of the dyes and the crystalline form of the nanoadsorbent [51–53]. As the structures become more crystalline, the intensity of the X-ray diffraction (XRD) peak increases. Consequently, when the LDH contains a higher amount of dye, the composite tends to become more amorphous and the intensity of the band decreases significantly. It is important to note that the crystalline structure is altered during the calcination process, resulting in the complete disappearance of the XRD peak. However, during rehydration, a significant recovery of the crystalline structure is observed. The curves of samples 4–6 have a low intensity due to the high dye load present in them, which results in a practically flat curve.

Analysing the XRD results further in a larger spectrum, we see a comparison of hydrotalcite before (H) and after calcination (HC) in Fig. 2. Analysing the H line we can see the diffraction peaks appearing at 11°, 23°, 34°, 34°, 39°, 46°, 60° and 61° which are, respectively, attributed to the crystalline planes 003, 006, 012, 015, 018, 110 and 113 [54]. After the calcination process there is a large variation of the peaks described

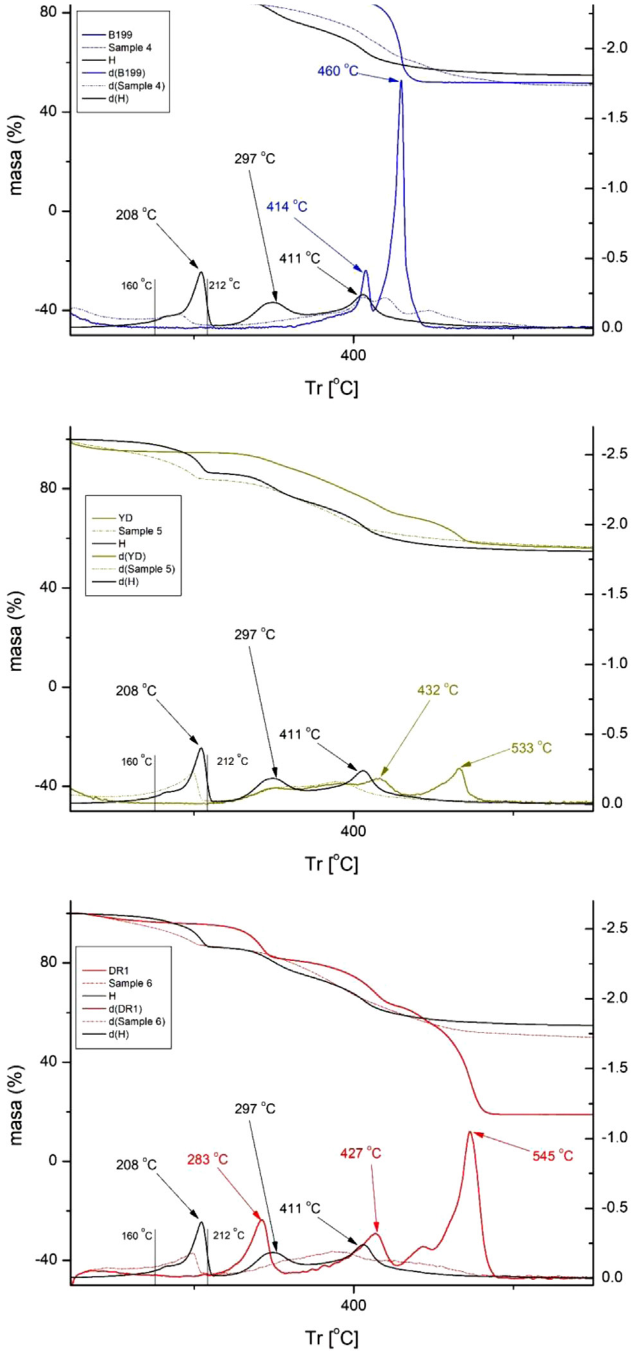

Fig. 6 – TGA and DTGA of for each dye, each hybrid and hydrotalcite.

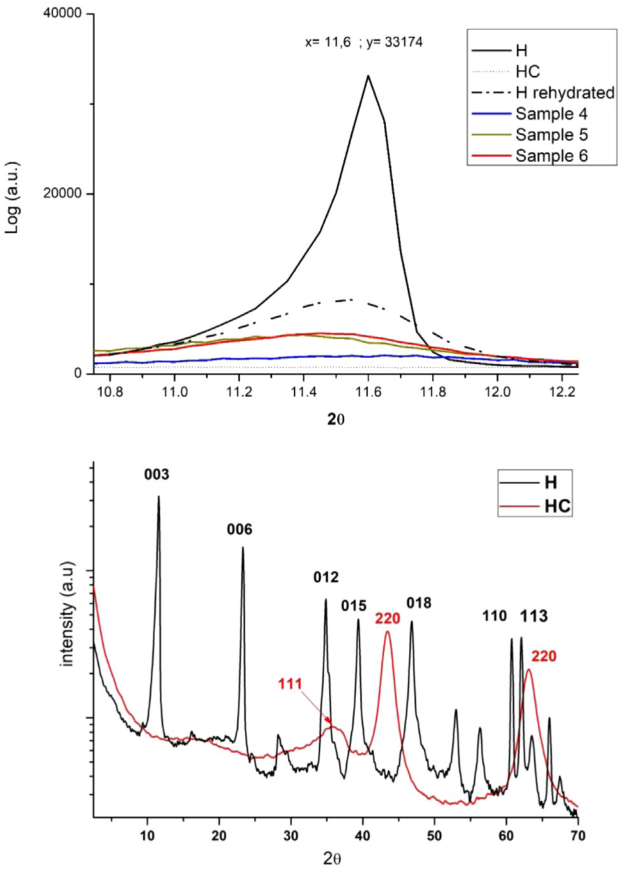

Fig. 7 – XRD for hydrotalcite, hydrotalcite calcinated, samples 4–6.

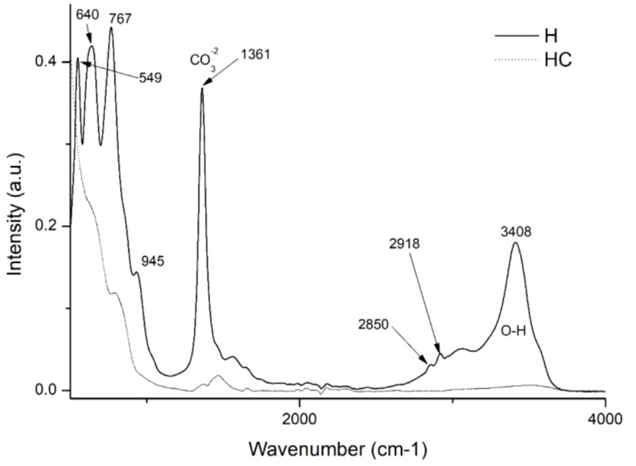

Fig. 8 – FTIR comparison of uncalcined hydrotalcite (H) and calcined hydrotalcite (HC).

above and diffraction peaks are seen showing an amorphous Mg(Al)O_X mixed oxide structure in the HC line [55].

Fourier transform infrared spectroscopy FTIR–ATR analysis

This instrumental technique will provide crucial information for the present study. The first objective is to investigate the impact of calcination on hydrotalcite. Fig. 8 shows two distinct bands: one at 1361 cm^{-1}, which is assigned to CO_3^{2-} [56,57] and a second band in the range 3200–3600 cm^{-1}, with a centre around 3408 cm^{-1}, which is attributed to the stretching of the —OH bond of interlaminar water [18,53,57]. In addition, two significant peaks are observed at 2850 and 2918 cm^{-1}, which are the result of stretching vibrations of the CH_2 group [58]. These bands disappear completely or weaken considerably after the calcination process, including the CO_3^{2-} band, indicating the possibility of incorporation of new anionic groups

Please cite this article in press as: D. López-Rodríguez, et al., Synthesis and characterisation of hybrids composed of calcined hydrotalcite and residual textile dyes, Bol. Soc. Esp. Cerám. Vidr. (2023), https://doi.org/10.1016/j.bsecv.2023.09.003

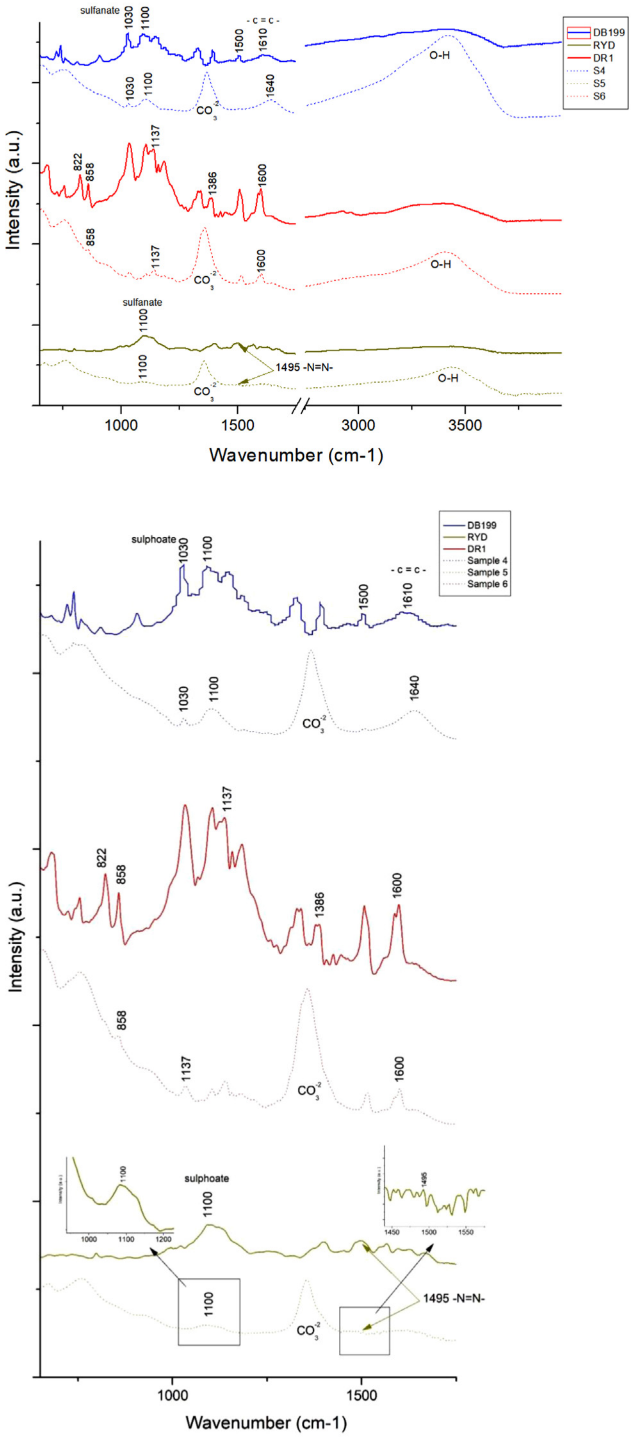

Fig. 9 – FTIR of DB199, RYD, DR1 and samples 4–6.

during subsequent rehydration. Other bands can be identified at 767 cm^{-1} related to the translation of the Al—OH group, at 640 cm^{-1} associated with the NO^{3-} and CO$_3$$^{2-}$ vibrations, and at 549 cm^{-1} related to the Mg—O bond vibrations [45,53].

The graphic representation presented in Fig. 9 illustrates the analysis of the spectra offered by each of the three dyes investigated in this study, as well as for their respective hybrids after subjecting them to adsorption with hydrotalcite. Upon close analysis, the hybrids exhibit distinctive clay-related features, such as a band identified at 1361 cm^{-1} corresponding to the CO$_3$$^{2-}$group, and another band located between 3200 and 3600 cm^{-1}, with a central peak at 3408 cm^{-1}, which is attributed to —OH bonds. It is particularly fascinating how these bands, previously lost during calcination, are recovered again after hydration and adsorption of the dyes, evidencing the structural memory present in this type of materials. Regarding the CO$_3$$^{2-}$ related band in sample 6, its presence is due to the fact that the dye used is of a non-ionic nature, resulting in a lower substitution of that group during the reconstruction process of the calcined clay.

When analyzing the area corresponding to DB199 and its hybrid sample 4, distinctive patterns can be observed in the spectrum. A prominent peak is recorded at 1100 cm^{-1}, which is attributed to the presence of compounds such as acetates, formates, propionates and benzoates [59]. Previous research works by different authors [51,52,56,58] have pointed out that the peaks found in the range of 1400–1640 cm^{-1} are related to the presence of benzene rings, while at 1030 and 1500 cm^{-1} characteristic vibrations of the sulfonate group [43] and the azo bond [60], respectively, are detected.

On the other hand, by examining the results of the RYD dye and its hybrid sample 5, certain functional groups can be identified in the spectrum. The sulfate groups are manifested through a peak at 1100 cm^{-1} [61,62] while the characteristic azo bond is observed at 1495 cm^{-1} [60].

In relation to the FTIR spectrum of Disperse Red 1, noticeable peaks are detected in different regions. For example, peaks are observed at 1600 cm^{-1} corresponding to the aromatic groups —C=C—. In addition, peaks at 1507 and 1341 cm^{-1} are recorded, which are attributed to asymmetric and symmetric stretching of the NO$_2$ functional group, respectively [63,64]. Other relevant peaks include those at 1386, 1142, 858 and 822 cm^{-1}, which originate from stretching of the —N=N— bond, stretching of the aliphatic —C—N— groups of the amine, out-of-plane bending of the C—H bond close to the NO$_2$ functional group, and out-of-plane bending of the aromatic C—H group, respectively [64].

X-ray photoelectron spectroscopy (XPS)

Fig. 10 and Table 5 present the binding energy values for various atoms that play a crucial role in the presence of both the LDH and the different dyes. The presence of C1s, O1s, Al2p3 and Mg1s at various peaks, such as 285, 530, 174 and 1308 eV respectively, confirms the presence of Hydrotalcite in all samples. In addition, the presence of N1s in the peak at 398 eV demonstrates the presence of nitrogen in each of the samples 4–6.

The figures also show that sample 4 exhibits peaks in the 932–945 eV range corresponding to Cu2p3, since the direct blue dye 199 contains copper in its structure. As for sample 5, which contains the yellow dye drimarene, the presence of sulphur is observed by a peak at 168.01 eV, which is attributed to S2p3.

Scanning Electron Microscopy Energy + Dispersive X-ray spectroscopy (SEM–EDX)

Energy dispersive analysis (EDX) was used to check for the presence of the constituent elements of the hybrids, the LDH

Please cite this article in press as: D. López-Rodríguez, et al., Synthesis and characterisation of hybrids composed of calcined hydrotalcite and residual textile dyes, Bol. Soc. Esp. Cerám. Vidr. (2023), https://doi.org/10.1016/j.bsecv.2023.09.003

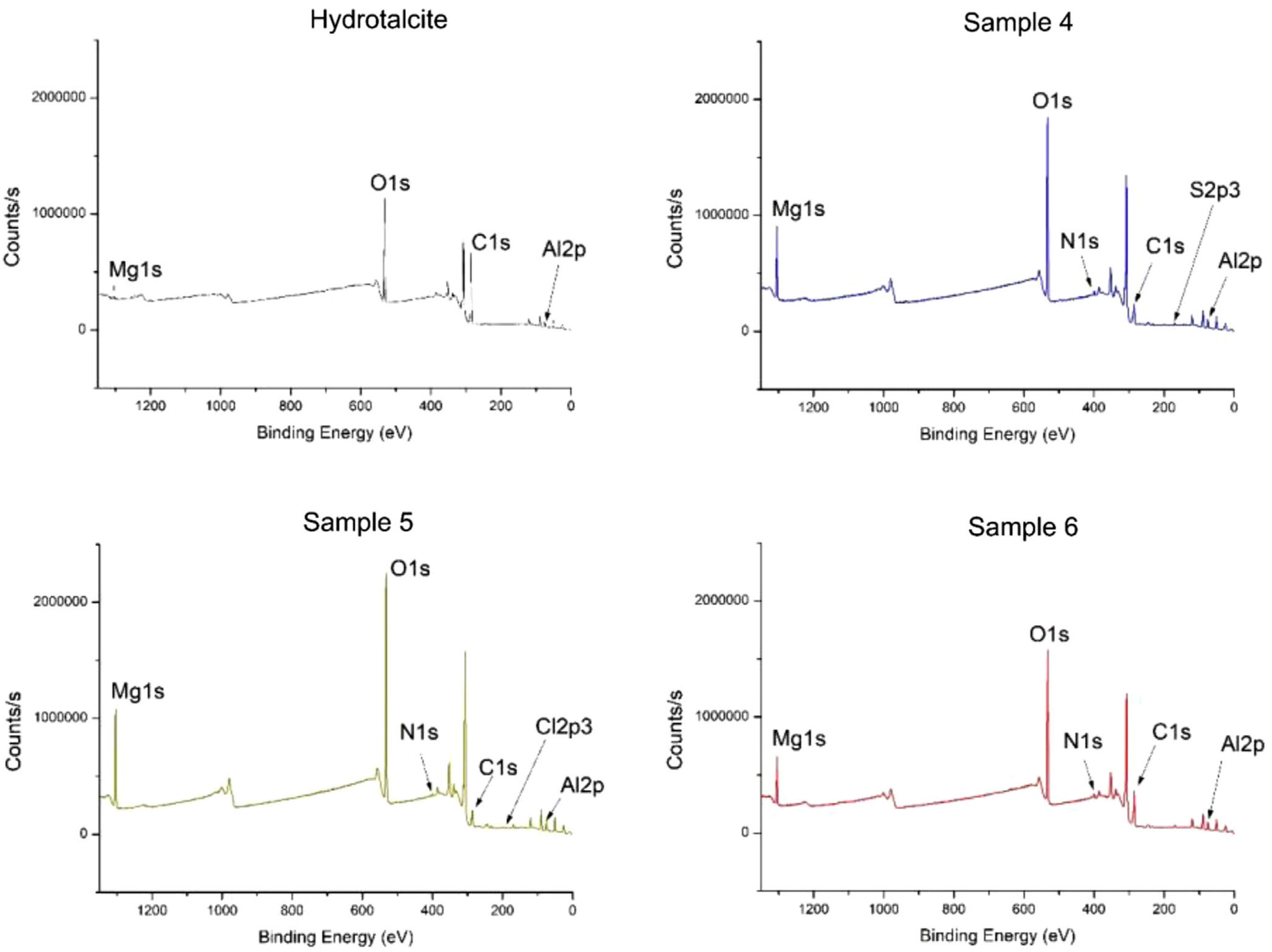

Fig. 10 – XPS hydrotalcite, samples 4–6.

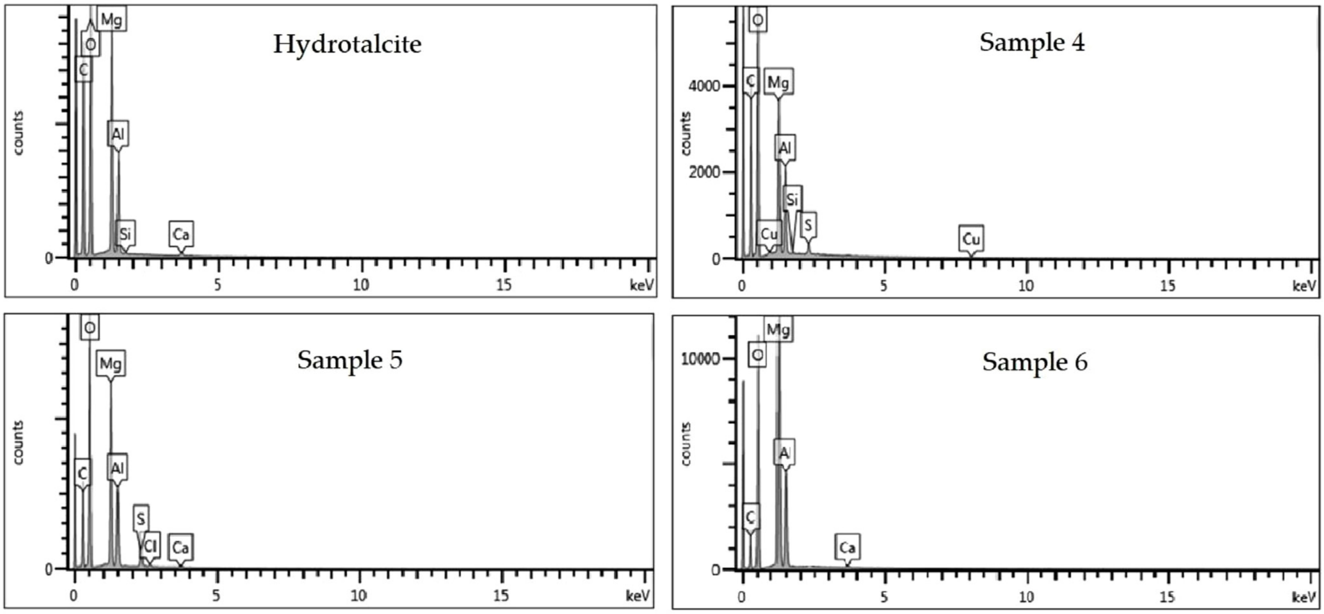

Fig. 11 – EDX hydrotalcite, samples 4–6.

Please cite this article in press as: D. López-Rodríguez, et al., Synthesis and characterisation of hybrids composed of calcined hydrotalcite and residual textile dyes, Bol. Soc. Esp. Cerám. Vidr. (2023), https://doi.org/10.1016/j.bsecv.2023.09.003

Table 5 – Binding energy H, samples.

C1s

Hydrotalcite				Sample 4				Sample 5				Sample 6			
B.E	FWHM eV	Area	%	B.E	FWHM eV	Area	%	B.E	FWHM eV	Area	%	B.E	FWHM eV	Area	%
284.56	1.1	121,809.04	85.68	284.64	1.41	32,377.81	51.39	297.38	1.43	24,452.58	48.57	284.61	1.46	67,532	68.39
285.22	1.02	7726	5.44	285.59	1.12	9590.51	15.22	297.38	1.18	4027.5	8.01	285.8	1.44	17,364.67	17.58
285.99	1.33	2552.77	1.80	286.47	1.6	7341.42	11.68	297.38	1.67	5891.23	11.74	287.14	2	4679.13	4.75
288.55	1.55	10,054.6	7.08	288.91	1.72	13,631.2	21.70	297.38	1.83	15,906.08	31.69	289.26	1.55	9139.44	9.28

O1s

Hydrotalcite				Sample 4				Sample 5				Sample 6			
B.E	FWHM eV	Area	%	B.E	FWHM eV	Area	%	B.E	FWHM eV	Area	%	B.E	FWHM eV	Area	%
530.29	1.56	39,229.75	11.89	530.86	1.56	86,427.73	15.12	530.7	1.49	89,079.44	13.38	530.9	1.56	61,928.33	13.38
531.49	1.68	278,048.9	84.29	532.09	1.68	464,049.21	81.28	531.75	1.7	556,751.48	83.72	531.98	1.71	383,308.49	82.93
532.81	1.59	12,566.04	3.82	533.4	1.59	20,556.34	3.60	532.47	1.99	19,292.66	2.91	533.37	1.59	17,051.09	3.69

Al2p3

Hydrotalcite				Sample 4				Sample 5				Sample 6			
B.E	FWHM eV	Area	%	B.E	FWHM eV	Area	%	B.E	FWHM eV	Area	%	B.E	FWHM eV	Area	%
73.82	1.47	9347.56	100	74.48	1.37	12,635.1	100	71.21	1.57	12,555.1	100	74.41	1.41	10,071.94	100

Mg1s

Hydrotalcite				Sample 4				Sample 5				Sample 6			
B.E	FWHM eV	Area	%	B.E	FWHM eV	Area	%	B.E	FWHM eV	Area	%	B.E	FWHM eV	Area	%
1308.68	1.57	61,905.82	100	1307.59	1.56	62,773.06	100	1312.44	1.54	121,327.91	100	1303.82	1.51	141,429.99	95.2
												1305.03	1.44	7617.21	5.1

N1s

Hydrotalcite				Sample 4				Sample 5				Sample 6			
B.E	FWHM eV	Area	%	B.E	FWHM eV	Area	%	B.E	FWHM eV	Area	%	B.E	FWHM eV	Area	%
–	–	–	–	398.65	1.5	9991.75	90.09	398.2	1.32	2056.41	30.95	399.34	1.94	10,913.85	86.34
				400.12	1.36	1098.18	9.91	399.6	1.43	3676.29	56.35	401.18	1.66	1730.72	13.66
								401.51	1.56	848.35	12.70				

S2p3

Hydrotalcite				Sample 4				Sample 5				Sample 6			
B.E	FWHM eV	Area	%	B.E	FWHM eV	Area	%	B.E	FWHM eV	Area	%	B.E	FWHM eV	Area	%
–	–	–	–					168.01	1.63	6512.31	100				

Cl2p3

Hydrotalcite				Sample 4				Sample 5				Sample 6			
B.E	FWHM eV	Area	%	B.E	FWHM eV	Area	%	B.E	FWHM eV	Area	%	B.E	FWHM eV	Area	%
–	–	–	–	–	–	–	–	197.51	1.3	1573.73	65.79	–	–	–	–
								199.99	1.42	826.37	34.21				

Cu2p3

Hydrotalcite				Sample 4				Sample 5				Sample 6			
B.E	FWHM eV	Area	%	B.E	FWHM eV	Area	%	B.E	FWHM eV	Area	%	B.E	FWHM eV	Area	%
–	–	–	–	932.8	1.95	2419.97	17.95	–	–	–	–	–	–	–	–
				934.98	1.54	5670.67	43.59								
				937.25	3.31	1554.34	12.82								
				942.19	3.36	1620.98	12.82								
				945.17	2.54	1661.52	12.82								

Please cite this article in press as: D. López-Rodríguez, et al., Synthesis and characterisation of hybrids composed of calcined hydrotalcite and residual textile dyes, Bol. Soc. Esp. Cerám. Vidr. (2023), https://doi.org/10.1016/j.bsecv.2023.09.003

Table 6 – BET surface areas, pore volumes and average pore sizes for hydrotalcite (H), hydrotalcite calcinated (HC), samples 4–6.

Sample	Surface area (m^2/g)	Pore volume (cm^3/g)	Average pore size (nm)
H	114.3	0.21	10.07
HC	239.6	0.37	18.7
4	102.2	0.15	11.8
5	109.8	0.14	12.8
6	101.1	0.17	11.6

and the different dyes. The spectra resulting from this analysis are presented in Fig. 11. From the known composition of the hydrotalcite, certain characteristic peaks are discovered at approximately 0.35, 0.5, 1.35, 1.5 and 1.85 keV, which correspond to the elements C, O, Mg, Al and Si, respectively. When analyzing the hybrid samples loaded with the dyes, the same peaks present in the hydrotalcite are identified, as well as new peaks confirming the presence of the respective dyes. In sample 4, a peak at 2.3 keV attributed to sulfur (S) and at approximately 8 keV attributable to copper (Cu) are detected. Moreover, in sample 5, the appearance of chlorine (Cl) can be evaluated due to the peak at 2.6 keV.

BET surface area and porosity measurements

A comprehensive BET analysis was performed to investigate the surface characteristics of the clay, as well as the size and depth of the corresponding pores, which are detailed in Table 6. A comparative study was carried out between the untreated hydrotalcite samples after calcination and after initial dye adsorption. The data compiled in Table 6 show significant changes in pore size and pore depth after calcination, which facilitates the entry and adsorption of the dye between the LDH layers. These findings are in agreement with previous studies that have also shown that these modifications are the result of catalyst outgassing due to the decomposition of gases present in the hydrotalcite into its hydrated phases [65–67]. By studying the nanoarsorbent after the adsorption process and subsequent rehydration to reconstruct its structure, very similar results to the initial ones are obtained, suggesting an effective recovery of the surface characteristics of the clay.

Conclusions

The adsorption capacity of hydrotalcite (H) for both anionic and non-ionic dyes has been successfully confirmed. The adsorption method involving calcination and subsequent reconstruction, utilising the shape memory properties of hydrotalcite, has been extensively studied and validated through XRD and FTIR tests. These analytical techniques, along with XPS and EDX, provide conclusive evidence of the presence of dyes within the hybrid structure. The XRD analysis reveals an increase in the amorphous region, confirming the incorporation of dyes, while the FTIR study demonstrates significant peaks corresponding to specific functional groups present in the dyes, such as amino and —SO_3— sulphonate groups.

Undoubtedly, the clay-dye hybrids offer great potential for the textile industry. With their favourable physical–chemical characteristics, these hybrids can be easily stored, transported, and handled. This opens up opportunities for collaboration between textile chemical manufacturers and dyeing companies, enabling the recovery of residual dyes from dye baths and subsequent synthesis of dye-loaded nanoadsorbents for commercial purposes. Furthermore, embracing such practices allows these manufacturers to enhance their commercial image and that of their customers by promoting the recycling and reuse of materials, thereby contributing to the principles of a circular economy.

REFERENCES

[1] S.M. Imtiazuddin, M. Mumtaz, K.A. Mallick, Pollutants of wastewater characteristics in textile industries, J. Basic Appl. Sci. 8 (2012) 554–556.

[2] S. Khan, A. Malik, Environmental and health effects of textile industry wastewater, Environ. Deterior. Hum. Heal. Nat. Anthropog. Determ. (2014) 55–71.

[3] R.B. Chavan, Indian Textile Industry-Environmental Issues, 2001.

[4] W. Trakarnpruk, S. Porntangjitlikit, Palm oil biodiesel synthesized with potassium loaded calcined hydrotalcite and effect of biodiesel blend on elastomer properties, Renew. Energy 33 (7) (2008) 1558–1563.

[5] D. Suescum-Morales, D.C. Fernández, J.M. Fernandez, J.R. Jimenez, The combined effect of CO_2 and calcined hydrotalcite on one-coat limestone mortar properties, Constr. Build. Mater. 280 (2021) 122532.

[6] P. Liu, M. Derchi, E.J.M. Hensen, Promotional effect of transition metal doping on the basicity and activity of calcined hydrotalcite catalysts for glycerol carbonate synthesis, Appl. Catal. B Environ. 144 (2014) 135–143.

[7] S. Carlino, Chemistry between the sheets, Chem. Br. 33 (9) (1997) 59–62.

[8] F. Bergaya, B.K.G. Theng, G. Lagaly, Developments in clay science, Handb. Clay Sci. 5 (2006) 1–19.

[9] F. Cavani, F. Trifiro, A. Vaccari, Hydrotalcite-type anionic clays: preparation, properties and applications, Catal. Today 11 (2) (1991) 173–301.

[10] M. Bouraada, M. Lafjah, M.S. Ouali, L.C. de Menorval, Basic dye removal from aqueous solutions by dodecylsulfate-and dodecyl benzene sulfonate-intercalated hydrotalcite, J. Hazard. Mater. 153 (3) (2008) 911–918.

[11] M.A. Ulibarri, I. Pavlovic, C. Barriga, M.C. Hermosın, J. Cornejo, Adsorption of anionic species on hydrotalcite-like compounds: effect of interlayer anion and crystallinity, Appl. Clay Sci. 18 (1–2) (2001) 17–27.

[12] D.L. Bish, Anion-exchange in takovite: applications to other hydroxide minerals, Bull. Miner. 103 (2) (1980) 170–175.

[13] S. Miyata, Physico-chemical properties of synthetic hydrotalcites in relation to composition, Clays Clay Miner. 28 (1) (1980) 50–56.

[14] M.-X. Zhu, Y.-P. Li, M. Xie, X. Hui-Zhen, Sorption of an anionic dye by uncalcined and calcined layered double hydroxides: a case study, J. Hazard. Mater. 120 (1–3) (2005) 163–171.

[15] M. Lakraimi, A. Legrouri, A. Barroug, J.P. Besse, Removal of pesticides from water by anionic clays, J. Chim. Phys. Physico-Chim. Biol. 96 (3) (1999) 470–478.

[16] T. Sato, K. Kato, T. Endo, M. Shimada, Preparation and chemical properties of magnesium aluminium oxide solid solutions, React. Solids 2 (3) (1986) 253–260.

[17] R. Salomao, L.M. Milena, M.H. Wakamatsu, V.C. Pandolfelli, Hydrotalcite synthesis via co-precipitation reactions using MgO and $Al(OH)_3$ precursors, Ceram. Int. 37 (8) (2011) 3063–3070.

[18] R.M.M. dos Santos, et al., Removal of Acid Green 68:1 from aqueous solutions by calcined and uncalcined layered double hydroxides, Appl. Clay Sci. 80–81 (2013) 189–195, http://dx.doi.org/10.1016/j.clay.2013.04.006.

[19] Z.Y. Lian, Z. Yang, X.Z. Wang, Manufacturing of high quality hydrotalcite by computational fluid dynamics simulation of an impinging jet crystallizer, Ceram. Int. (2022), http://dx.doi.org/10.1016/J.CERAMINT.2022.02.081.

[20] X.-J. Xiong, X.-J. Meng, T.-L. Zheng, Biosorption of CI Direct Blue 199 from aqueous solution by nonviable *Aspergillus niger*, J. Hazard. Mater. 175 (1–3) (2010) 241–246.

[21] M. Laqbaqbi, M.C. García-Payo, M. Khayet, J. El Kharraz, M. Chaouch, Application of direct contact membrane distillation for textile wastewater treatment and fouling study, Sep. Purif. Technol. 209 (August 2018) (2019) 815–825, http://dx.doi.org/10.1016/j.seppur.2018.09.031.

[22] L. da Silva Leite, B. de Souza Maselli, G. de Aragão Umbuzeiro, R.F. Pupo Nogueira, Monitoring ecotoxicity of disperse red 1 dye during photo-Fenton degradation, Chemosphere 148 (2016) 511–517.

[23] J.L. Bigman, Monitoring of chemicals and water, Handb. Silicon Wafer Clean. Technol. (2018) 619–657, http://dx.doi.org/10.1016/B978-0-323-51084-4.00011-3.

[24] M.M.F. Silva, M.M. Oliveira, M.C. Avelino, M.G. Fonseca, R.K.S. Almeida, E.C. Silva Filho, Adsorption of an industrial anionic dye by modified-KSF-montmorillonite: evaluation of the kinetic, thermodynamic and equilibrium data, Chem. Eng. J. 203 (2012) 259–268, http://dx.doi.org/10.1016/j.cej.2012.07.009.

[25] B. Micó-Vicent, F.M. Martínez-Verdú, Method for optimising the synthesis of hybrid nanopigments. ES2568833A1 Patent, 2017.

[26] H. Fischer, L.F. Batenburg, Coloring Pigment.

[27] C. Mensch, R. Chintala, D. Nawrocki, J.T. Blue, A. Bhambhani, Enabling lyophilized pneumococcal conjugate vaccines through formulation design and excipient selection suitable for a multivalent adjuvanted vaccine, J. Pharm. Sci. (2020) 1–11, http://dx.doi.org/10.1016/j.xphs.2020.10.038.

[28] L.S. Castillo-Peinado, M. Calderón-Santiago, F. Priego-Capote, Lyophilization as pre-processing for sample storage in the determination of vitamin D3 and metabolites in serum and plasma, Talanta 222 (September 2020) (2021), http://dx.doi.org/10.1016/j.talanta.2020.121692.

[29] S. Maharjan, K.S. Liao, A.J. Wang, S.A. Curran, Highly effective hydrophobic solar reflective coating for building materials: increasing total solar reflectance via functionalized anatase immobilization in an organosiloxane matrix, Constr. Build. Mater. 243 (2020) 118189, http://dx.doi.org/10.1016/j.conbuildmat.2020.118189.

[30] C. Di Natale, D. Monti, R. Paolesse, Chemical sensitivity of porphyrin assemblies, Mater. Today 13 (7–8) (2010) 46–52.

[31] Y. Liu, et al., Separation and identification of microplastics in marine organisms by TGA–FTIR–GC/MS: a case study of mussels from coastal China, Environ. Pollut. (2020) 115946, http://dx.doi.org/10.1016/j.envpol.2020.115946.

[32] M. Umar, M.I. Ofem, A.S. Anwar, A.G. Salisu, Thermo gravimetric analysis (TGA) of PA6/G and PA6/GNP composites using two processing streams, J. King Saud. Univ.-Eng. Sci. (2020), http://dx.doi.org/10.1016/j.jksues.2020.09.003.

[33] I. Corazzari, F. Turci, R. Nisticò, TGA coupled with FTIR gas analysis to quantify the vinyl alcohol unit content in ethylene-vinyl alcohol copolymer, Mater. Lett. 284 (2021) 129030, http://dx.doi.org/10.1016/j.matlet.2020.129030.

[34] H. Pálková, et al., Laponite-derived porous clay heterostructures: I. Synthesis and physicochemical characterization, Micropor. Mesopor. Mater. 127 (3) (2010) 228–236, http://dx.doi.org/10.1016/j.micromeso.2009.07.019.

[35] W. Zhuo, Y. Xie, M.T. Benson, J. Ge, R.D. Mariani, J. Zhang, XRD and SEM/EDS characterization of two quaternary fuel alloys (U–2.5Mo–2.5Ti–5.0Zr and U–1.5Mo–1.5Ti–7.0Zr in wt.%) for fast reactors, Mater. Charact. 170 (September) (2020) 110696, http://dx.doi.org/10.1016/j.matchar.2020.110696.

[36] B. Li, Y. Zhang, X. Zhou, Z. Liu, Q. Liu, X. Li, Different dye removal mechanisms between monodispersed and uniform hexagonal thin plate-like MgAl–$CO_3{}^{2-}$-LDH and its calcined product in efficient removal of Congo red from water, J. Alloys Compd. 673 (2016) 265–271.

[37] C. Zhang, S. Yang, H. Chen, H. He, C. Sun, Adsorption behavior and mechanism of reactive brilliant red X-3B in aqueous solution over three kinds of hydrotalcite-like LDHs, Appl. Surf. Sci. 301 (2014) 329–337.

[38] R.-r. Shan, et al., Highly efficient removal of three red dyes by adsorption onto Mg–Al-layered double hydroxide, J. Ind. Eng. Chem. 21 (2015) 561–568.

[39] E. Heraldy, S.J. Santosa, T. Triyono, K. Wijaya, Anionic and cationic dyes removal from aqueous solutions by adsorption onto synthetic Mg/Al hydrotalcite-like compound, Indones. J. Chem. 15 (3) (2015) 234–241.

[40] F. Grum, R.F. Witzel, P. Stensby, Evaluation of whiteness, JOSA 64 (2) (1974) 210–215.

[41] ASTM, Standard tables for reference solar spectral irradiances: direct normal and hemispherical on 37° tilted surface, ASTM 03 (Reapproved) (2013) 1–21, http://dx.doi.org/10.1520/G0173-03R20.2.

[42] J.L. Iturbe-García, J.B. Martínezs, F.G. Correa, B.E. López-Muñoz, Behavior of a hydrotalcite type material obtained from MgAl alloy for CO_2 adsorption, Appl. Clay Sci. 183 (2019) 105296, http://dx.doi.org/10.1016/j.clay.2019.105296.

[43] R. Extremera, I. Pavlovic, M.R. Pérez, C. Barriga, Removal of acid orange 10 by calcined Mg/Al layered double hydroxides from water and recovery of the adsorbed dye, Chem. Eng. J. 213 (2012) 392–400, http://dx.doi.org/10.1016/j.cej.2012.10.042.

[44] Q. Wang, Y. Feng, J. Feng, D. Li, Enhanced thermal- and photo-stability of acid yellow 17 by incorporation into layered double hydroxides, J. Solid State Chem. 184 (6) (2011) 1551–1555, http://dx.doi.org/10.1016/j.jssc.2011.04.020.

[45] T. Lopez, P. Bosch, M. Asomoza, R. Gómez, E. Ramos, DTA–TGA and FTIR spectroscopies of sol–gel hydrotalcites: aluminum source effect on physicochemical properties, Mater. Lett. 31 (3–6) (1997) 311–316.

[46] S.K. Ghosh, et al., Rhodamine 6G Intercalated Montmorillonite Nanopigments-Polyethylene Composites: Facile Synthesis and Ultravioletstability Study, 2011.

[47] S. Raha, I. Ivanov, N.H. Quazi, S.N. Bhattacharya, Photo-stability of rhodamine-B/montmorillonite nanopigments in polypropylene matrix, Appl. Clay Sci. 42 (3–4) (2009) 661–666.

[48] F. Bellucci, G. Camino, A. Frache, A. Sarra, Catalytic charring-volatilization competition in organoclay nanocomposites, Polym. Degrad. Stab. 92 (3) (2007) 425–436.

[49] A. Landau, A. Zaban, I. Lapides, S. Yariv, Montmorillonite treated with rhodamine-6G mechanochemically and in

Please cite this article in press as: D. López-Rodríguez, et al., Synthesis and characterisation of hybrids composed of calcined hydrotalcite and residual textile dyes, Bol. Soc. Esp. Cerám. Vidr. (2023), https://doi.org/10.1016/j.bsecv.2023.09.003

aqueous suspensions, J. Therm. Anal. Calorim. 70 (1) (2002) 103–113.

[50] E. Dahdah, J. Estephane, Y. Taleb, B. El Khoury, J. El Nakat, S. Aouad, The role of rehydration in enhancing the basic properties of Mg–Al hydrotalcites for biodiesel production, Sustain. Chem. Pharm. 22 (July) (2021), http://dx.doi.org/10.1016/j.scp.2021.100487.

[51] E. Bernard, W.J. Zucha, B. Lothenbach, U. Mäder, Stability of hydrotalcite (Mg–Al layered double hydroxide) in presence of different anions, Cem. Concr. Res. 152 (2022) 106674, http://dx.doi.org/10.1016/J.CEMCONRES.2021.106674.

[52] A. Geetha Bhavani, T.A. Wani, A. Ma'Aruf, T. Prasad, Effect of ageing process on crystal morphology of Co–Mg–Al hydrotalcite, Mater. Today Proc. 44 (2021) 2277–2282, http://dx.doi.org/10.1016/J.MATPR.2020.12.390.

[53] B. Wiyantoko, P. Kurniawati, T.S. Purbaningtias, I. Fatimah, Synthesis and characterization of hydrotalcite at different Mg/Al molar ratios, Proc. Chem. 17 (2015) 21–26.

[54] A. Serrano-Lotina, L. Rodríguez, G. Muñoz, A.J. Martin, M.A. Folgado, L. Daza, Biogas reforming over La–NiMgAl catalysts derived from hydrotalcite-like structure: Influence of calcination temperature, Catal. Commun. 12 (11) (2011) 961–967, http://dx.doi.org/10.1016/J.CATCOM.2011.02.014.

[55] B. Micó-Vicent, J. Jordán, E. Perales, F. Martínez-Verdú, F. Cases, Finding the additives incorporation moment in hybrid natural pigments synthesis to improve bioresin properties, Coatings 9 (2019). doi:10.3390/coatings9010034.

[56] J.C.A.A. Roelofs, J.A. van Bokhoven, A. Jos Van Dillen, J. Geus, K.P. de Jong, The thermal decomposition of Mg–A1 hydrotalcites: effects of interlayer anions and charateristics of the final structure, Chem. Eur. J. 8 (2002) 5571–5579.

[57] H. Ziyat, S. Elmzioui, M.N. Bennani, J. Houssaini, S. Allaoui, S. Arhzaf, Kinetic, isotherm, and mechanism investigations of the removal of nitrate and nitrite from water by the synthesized hydrotalcite Mg–Al, Res. Chem. Intermed. 47 (6) (2021) 2605–2627.

[58] Y. Ma, J. Zhu, H. He, P. Yuan, W. Shen, D. Liu, Infrared investigation of organo-montmorillonites prepared from different surfactants, Spectrochim. Acta A Mol. Biomol. Spectrosc. 76 (2) (2010) 122–129.

[59] M.K. Hafshejani, C.J. Ogugbue, N. Morad, Application of response surface methodology for optimization of decolorization and mineralization of triazo dye Direct Blue 71 by *Pseudomonas aeruginosa*, 3 Biotech. 4 (6) (2014) 605–619, http://dx.doi.org/10.1007/s13205-013-0192-7.

[60] C. Hu, C. Yu Jimmy, Z. Hao, P.K. Wong, Photocatalytic degradation of triazine-containing azo dyes in aqueous TiO_2 suspensions, Appl. Catal. B Environ. 42 (1) (2003) 47–55.

[61] K.W. Evanson, M.W. Urban, Surface and interfacial FTIR spectroscopic studies of latexes. I. Surfactant–copolymer interactions, J. Appl. Polym. Sci. 42 (8) (1991) 2287–2296.

[62] R. Seoudi, G.S. El-Bahy, Z.A. El Sayed, FTIR, TGA and DC electrical conductivity studies of phthalocyanine and its complexes, J. Mol. Struct. 753 (1–3) (2005) 119–126.

[63] Y. Cui, M. Wang, L. Chen, G. Qian, Synthesis and spectroscopic characterization of an alkoxysilane dye containing C. I. Disperse Red 1, Dye Pigment. 62 (1) (2004) 43–47, http://dx.doi.org/10.1016/J.DYEPIG.2003.11.009.

[64] H. Taunaumang, H. Herman, M.O. Tjia, Molecular orientation in Disperse Red 1 thin film produced by PVD method, Opt. Mater. (Amst.) 18 (3) (2001) 343–350, http://dx.doi.org/10.1016/S0925-3467(01)00169-0.

[65] D. Tichit, et al., Textural properties and catalytic activity of hydrotalcites, J. Catal. 151 (1) (1995) 50–59.

[66] Y. Liu, E. Lotero, J.G. Goodwin, X. Mo, Transesterification of poultry fat with methanol using Mg–Al hydrotalcite derived catalysts, Appl. Catal. A Gen. 331 (1) (2007) 138–148, http://dx.doi.org/10.1016/j.apcata.2007.07.038.

[67] J. Shen, M. Tu, C. Hu, Structural and surface acid/base properties of hydrotalcite-derived MgAlO oxides calcined at varying temperatures, J. Solid State Chem. 137 (2) (1998) 295–301, http://dx.doi.org/10.1006/jssc.1997.7739.

Please cite this article in press as: D. López-Rodríguez, et al., Synthesis and characterisation of hybrids composed of calcined hydrotalcite and residual textile dyes, Bol. Soc. Esp. Cerám. Vidr. (2023), https://doi.org/10.1016/j.bsecv.2023.09.003